

Neutron-based techniques for archaeometry: characterization of a Sardinian boat model

Questa è la versione Post print del seguente articolo:

*Original*

Neutron-based techniques for archaeometry: characterization of a Sardinian boat model / Depalmas, A.; Cataldo, M.; Grazi, F.; Scherillo, A.; Fedrigo, A.; Kockelmann, W.; di Gennaro, F.; Canu, A.; Brunetti, A.. - In: ARCHAEOLOGICAL AND ANTHROPOLOGICAL SCIENCES. - ISSN 1866-9557. - 13:6(2021), pp. 1-9. [10.1007/s12520-021-01345-w]

*Availability:*

This version is available at: 11388/246878 since: 2021-05-24T18:02:44Z

*Publisher:*

*Published*

DOI:10.1007/s12520-021-01345-w

*Terms of use:*

Chiunque può accedere liberamente al full text dei lavori resi disponibili come "Open Access".

*Publisher copyright*

note finali coverpage

(Article begins on next page)



# Neutron-based techniques for archaeometry: characterization of a Sardinian boat model

A. Depalmas<sup>1</sup> · M. Cataldo<sup>2,3</sup> · F. Grazzi<sup>4</sup> · A. Scherillo<sup>3</sup> · A. Fedrigo<sup>3</sup> · W. Kockelmann<sup>3</sup> · F. di Gennaro<sup>5</sup> · A. Canu<sup>5</sup> · A. Brunetti<sup>2</sup>

Received: 18 January 2021 / Accepted: 12 April 2021  
© The Author(s) 2021

## Abstract

Sardinian metallurgy produced samples of high artistic and historical value. In particular, ship models are rare and unmatched examples of the mastery reached by Sardinian metallurgists and their production process deserves an in-depth analysis of all the phases involved in the making. In this work, we examined a Sardinian boat model to obtain information about its composition, microstructure and manufacturing technique. The object is a small bronze ship model that was found near the Nuraghe Colovros, located in north-east Sardinia (Italy). It was analysed by means of neutron imaging and neutron diffraction experiments at the ISIS Pulsed Neutron and Muon Source laboratory (Harwell, UK). Neutron techniques are relatively new in the field of archaeometry, but they are a very effective tool for the study of archaeological objects: they permit to survey complete artefacts, determine compositions and structures, assess the conservation status and address questions of effective use and casting techniques. This type of data can add new and different insights to existing archaeological information, especially where sampling is not permitted. The outcome of the study reveals a peculiar approach to the manufacturing of the boat model.

**Keywords** Neutron imaging · Neutron diffraction · Boat model · Sardinian bronze casting · Non-destructive analysis

## Introduction

Sardinian bronze artefacts constitute a rich historical archive providing key information about the metal production and casting techniques concerning the development of metallurgy in the Mediterranean area. The island is rich in metal ores: yet, the exploitation of these resources was not constant during prehistoric times. Ornamental elements and small silver or copper utensils appeared at the

end of the Neolithic and in the Copper Age, while evidence of the use of bronze alloys is attested at the beginning of the Bronze Age. It is in the Final Bronze Age (12<sup>th</sup>–10<sup>th</sup> Century BC) and the Early Iron Age (10<sup>th</sup>–7<sup>th</sup> Century BC), however, that the metallurgical activity has a significant development. Sardinian metallurgy, therefore, mostly developed in a period that, according to the most recent proposals, is preferentially post-Nuragic than “Nuragic” time; it refers to a period (Final Bronze and Early Iron Age) in which *nuraghi* were no longer built and there was a significant change in social organization (Depalmas 2019). The large circulation of ingots, whole or in pieces, often found in hoards, and the identification of metal artefacts workshops, particularly in the villages surrounding sanctuaries, suggest that the great development of metallurgy is directly connected with the new society that created and managed the great centres of aggregation represented by places of worship (sacred wells and springs, megaron temples, etc.) where weapons, tools and figured bronzes were offered (Depalmas et al. 2016). During this period, numerous categories of tools and weapons were produced, as well as figurative bronzes, i.e. small bronze figures depicting men and women,

✉ M. Cataldo  
Matteo.Cataldo@stfc.ac.uk

<sup>1</sup> Dipartimento di Scienze Umanistiche e Sociali, Università degli Studi di Sassari, Sassari, Italy

<sup>2</sup> Dipartimento di Chimica e Farmacia, Università degli Studi di Sassari, Sassari, Italy

<sup>3</sup> Science and Technology Facility Council (STFC), ISIS Pulsed Neutron and Muon Source, Harwell, UK

<sup>4</sup> CNR, Istituto di Fisica Applicata “Nello Carrara”, Sesto Fiorentino, Italy

<sup>5</sup> Soprintendenza Archeologia, Belle Arti e Paesaggio di Sassari e Nuoro, Sassari, Italy

objects, animals and boat models. Boat/ship models, in particular, are the miniature representation of their larger siblings and represent a very specific type of objects that testify the special bond between the Sardinian Iron Age culture and the sea. So far, more than 200 boat models have been discovered and recorded. In most of the recorded samples, there are three main aspects that characterize Sardinian boat models: a hull with a typical biconvex or circular shape; an animal head on the top of the bowsprit (*protome*); and a bridge with a ring on its top that connects the two sides of the hull. Besides, animal figurines on the boat deck and/or mainmasts are decorations recurrent in some boats featuring complex scenes. To date, it is not possible to give a clear definition of their purpose, because a lot depends on the finding context. Still, since boat models were generally found in religious contexts, the accepted theory among the archaeological community is that they probably served as votive lamps (Depalmas 2014). With regard to manufacturing, it is well known that these types of artefacts were made in bronze by the lost wax method. However, when dealing with a complex sample shape, some problems could arise during the casting process, as the difficulty of the molten metal to fill up the whole mould volume. Furthermore, one of the main issues concerns the connection between the different elements of the boat, since it is assumed that metallurgists of the first Iron Age were not able to make soldering (Lechtman and Steinberg 1980). This assumption leads to hypothesize that complex shapes as animal figurines and other decorations might have been added at a second stage, on top of a first casting of the hull and the *protome*, by using the casting-on technique (Brunetti and Al 2018). Following this procedure, the joint was made by putting the wax model of decorative elements directly on the pre-casted hull and by building up the mould around it. Then, the molten bronze was directly poured into the mould and the added element was automatically connected to the main body by solidifying on it. The bond originated by this method is very strong, and the connected parts appear as a single one. This work aims to characterize the elemental and phase compositions of the Colovros boat and to establish whether it was made in a single casting or, as in the case of more complex examples, it was made using the casting-on technique.

## Materials and methods

The boat model was found near Nuraghe Colovros in the territory of Lula, north-east Sardinia (Depalmas et al. forthcoming). As evident from Fig. 1, the object recalls all the standard elements of a Sardinian Iron Age boat model. A detailed description of the boat is reported in Table 1. The



**Fig. 1** The boat from Colovros Nuraghe. It was found in the territory of Lula, north-east Sardinia

boat was analysed by using two different neutron techniques: neutron tomography (NT) and time-of-flight neutron diffraction (ToF-ND) at ISIS Pulsed Neutron and Muon Source. NT was performed on the IMAT imaging station (Imaging and Materials science) Kockelmann W. and Al (2018) while ToF-ND was applied on the INES Station (Italian Neutron Experimental Station) (Imberti et al. 2008). Neutron tomography and neutron diffraction provide complementary information for the characterization of metallic materials properties in a non-destructive approach, which is almost mandatory when dealing with a work of art or archaeological artefacts (Kardijlov and Festa 2017).

## The neutron imaging instrument—IMAT

IMAT is a cold neutron imaging instrument for attenuation-based transmission measurements (neutron radiography and tomography) and energy-resolved neutron imaging (Kockelmann and Al 2018). For this measurement, we used the IMAT natural neutron bandwidth (1–6 Å) and we acquired transmission images using the 2048 × 2048 pixels ANDOR Zyla sCMOS 4.2 PLUS camera coupled to a ZnS/LiF scintillator screen. The instrument is equipped with a heavy-duty x-y-z- $\omega$  rotation stage for samples up to 1.5 t (Fig. 2). The achievable spatial resolution due to geometrical image unsharpness depends on the so-called  $L/D$  ratio, where  $L$  is the pinhole-detector distance and  $D$  is the pinhole diameter. The pinhole selector is placed 10 m from the camera and offers five different apertures for defining the  $L/D$  ratio. The “pinhole” is a neutron collimator that produces an almost parallel neutron beam. By changing the beam incident divergence (i.e. the pinhole diameter  $D$ ) the image sharpness can be tuned. For our set-up, we used a pinhole size of 40 mm, while  $L$  is 10 m, giving an  $L/D$  of 250. To minimize the image blurring, the sample was positioned as close as possible to the detector. Neutron tomography was performed on the boat as a first experimental step, to gain details about its morphology and therefore drive the

**Table 1** Archaeological description of the Colovros boat (Depalmas 2005)

Provenance	Colovros, Lula (NU), Italy—Surface find Nicolò Sanna, 2017
Description	The boat belongs to the type 2 “Ghilarza” classification (Depalmas 2005). It is a bronze boat with a biconvex hull, sharp stem and straight sides with three relief ribbings at different heights. A bridge with edges and a ring on top connects the two sides of the hull. The bottom of the keel is flat, with four little conical feet. The bowsprit is characterized by an animal “protome” (head) representing a bovine with a short neck covered by a spiral wrapping. The snout has a cylindrical shape; the ears are small, placed under the curved horns while the eyes are spherical
State of conservation	Good. The front left foot and the right horn are partly broken
Dimensions	Total length, 13.5 cm; hull length, 11.4 cm; maximum width, 4.8 cm; hull height, 2.0 cm; hull thickness, 3 mm
Chronology	Early Iron Age

selection of areas of interest for the diffraction measurements. To position the boat on the IMAT rotating stage, for the measurement of angular projections to perform tomography reconstruction, it was wrapped in aluminium foil (a material almost transparent to neutrons) and inserted into an aluminium cylinder mounted on the rotating stage. Since we aimed at a spatial resolution of 110  $\mu\text{m}$  allowing for the IMAT medium-resolution field of view ( $112.7 \times 112.7 \text{ mm}^2$ ), the length of the boat did not fit completely inside a single neutron radiograph, but it was necessary to vertically translate the sample. So, two sets of projections with corresponding angular positions but different vertical heights were acquired. Each scan consisted of 1347 projection angles over  $360^\circ$ , acquired for 30 s to maximize the contrast generated by the attenuation of the neutron beam induced by the sample. A set

of 20 direct beam measurements (with no object) and a set of 20 dark current measurements (with no neutrons) were also taken for normalization purposes. Image filtering for gamma white spot removal was performed using ImageJ (Ruenden and Al 2017), and normalization was performed using the Octopus Reconstruction software (Dierick et al. 2014). Before reconstructing the 3D volume, we stitched the two sets of normalized projections using a dedicated plugin of ImageJ (Preibisch et al. 2009). Tomographic reconstruction was performed using a parallel-beam filtered back-projection algorithm in Octopus (Kak 2001). The obtained stack of images represents a three-dimensional matrix of the attenuation coefficients of the sample, generally represented in grayscale levels where high attenuating parts are visualized as bright/white areas and more transparent materials as dark/black ones.

**Fig. 2** The IMAT imaging station

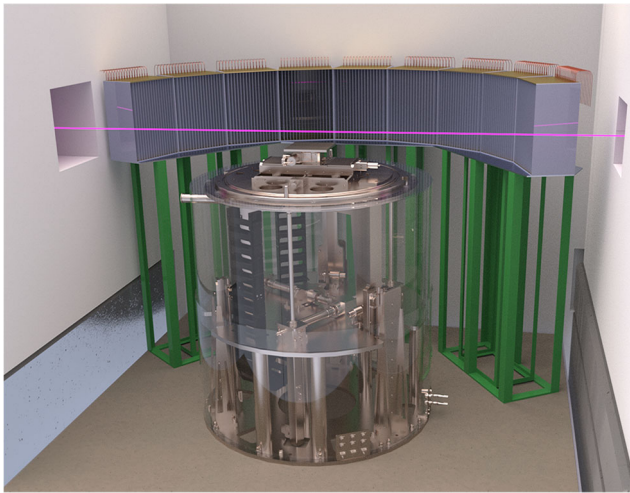


**Fig. 3** 3D render of INES instrument environment

### The neutron diffraction instrument—INES

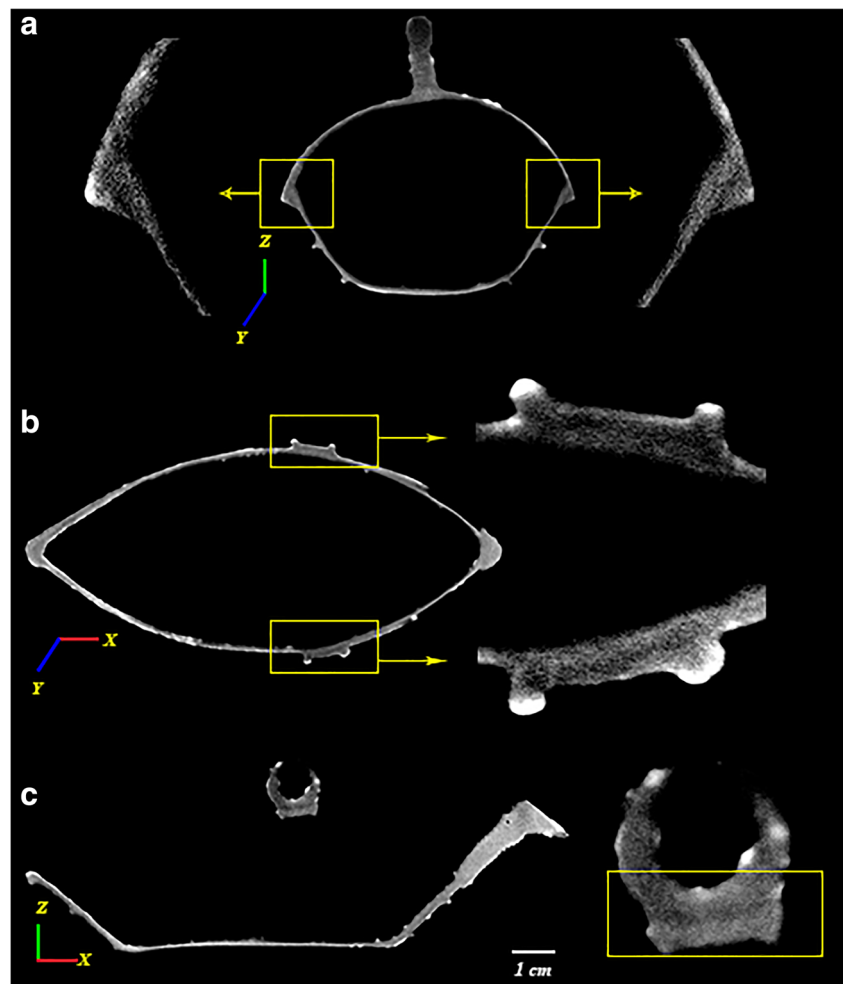
INES is a time-of-flight neutron diffractometer with detectors at fixed scattering angles and corresponding diffraction patterns with neutron counts as a function of time. The average flux on the INES sample position is about  $10^6$  n/cm<sup>2</sup>/s (Grazzi et al. 2007). The instrument is equipped with several features that allow for accurate positioning and analysis of samples with complex shape: an x-y-z- $\omega$  table in the sample area, used for moving and orienting the sample with respect to the neutron beam (Fig. 3), and a set of boron carbide enriched ceramic jaws, to shape the incident neutron beam and modify the size of the irradiated area (Celli et al. 2007). ToF-ND was performed on the boat after the NT measurements. The boat was mounted on the table and measured in thirteen different points, obtaining a complete characterization and phase mapping of a significant portion of the entire structure. Each measurement point was decided depending on the morphology of the sample, through a visual inspection, and by inspecting the virtual volume reconstructed from the neutron tomography. The irradiated area cross-sections ranged from 9 mm<sup>2</sup> to 150 mm<sup>2</sup>. Diffraction data were processed with the Mantid code (Arnold and Al 2014) and refined through the Rietveld refinement method (McCusker et al. 1999) using the GSAS software (Larson 2004) through the EXPGUI interface (Toby 2001). The Rietveld analysis allowed to quantify the different metal (face-centred cubic phase containing copper-tin substitutional alloy and face-centred cubic phase of lead) and mineral phases (cuprite, nantokite, chalcocite) present in the artefact. The diffraction peak profile analysis of the metal phases was, instead, performed to obtain information regarding the production techniques (Grazzi 2018).

## Results

### Neutron tomography

In the following paragraphs, the results of the neutron-based analysis are reported. One of the main questions regarding the manufacturing is the possibility of the separate casting of different parts of the boat, especially the more challenging areas to make, such as the ring, the bridge and the *protome*. These parts could have been added in a second stage using the casting-on technique, as reported in Brunetti and Al (2018) for the Vetulonia boat. Figure 4 reports three different slices of the boat with zoomed section. The sections were selected to display the specific areas where the different parts of the boat connect together. A detailed analysis of these slices revealed the presence of discontinuities, especially at the bridge-hull (4A-B) and ring-bridge connections (4C). As shown in the zoomed sections, in these regions, a darker area is visible, i.e. a change in the attenuation of the beam where the connection occurs. In Fig. 4A, it is possible to see how the bridge is installed upon the hull: if the boat were made in a single cast, the structure would have been continuous, while, in this case, we are able to distinguish a discontinuity. This hypothesis is confirmed by Fig. 4B, which reports the same junction area on the XY plane: by enhancing the contrast in the zoomed section, it is possible to determine the same situation as Fig. 4A. Finally, Fig. 4C reports a slice of the XZ plane, where we are also able to distinguish a discontinuity at the ring-bridge connection. The ring, eventually, is the third part that constitutes the boat. Addressing the time order of the casting of these parts is not an easy task but, by comparing the results of neutron imaging with the results of neutron diffraction in the next paragraph, we can hypothesize how the manufacturing of the boat happened. Another important detail observed in the neutron imaging data is the presence of pores within the metal structure. Pores are small air pockets that are formed during casting, due to the presence of gasses trapped into the molten metal or as a consequence of the cooling of the metal in the mould (Fig. 5). The presence of pores may be detrimental to the mechanical properties of the metal object since such defects within the structure are less resistant to external stresses. Figure 5 also reports a very interesting detail of the metal structure. Just underneath the pore, it is possible to distinguish differences in the grey tones, with lighter and darker areas. This can be ascribed to a locally different Sn content of the Cu-Sn phase, showing the presence of localized dendrites. Furthermore, from this picture, it is possible to assess that the “wire” surrounding the neck is part of the primary metal structure. Finally, Fig. 6 reports a projection of the entire boat, obtained by adding all the

**Fig. 4** Three different slices of the boat with specific zoomed areas are reported. The slices were selected to emphasize the connection areas. Figure 4A, taken on the YZ plane, gives a clear indication of what is described as “discontinuities”. As shown in the zoomed section (left and right), it is possible to see how the bridge of the boat makes the connection with the hull, giving rise to a discontinuity (darker area) at the joint section. The same consideration can be done also for Fig. 4B, which is taken in the XY plane. Figure 4C, taken in the XZ plane, considers the third part of the boat, the ring, which was the last part to be connected: a clear discontinuity in the form of a darker area at the joint section is visible in the zoomed ring



slices on the XZ plane. In the projection, bright spots are visible within the structure. These areas correspond to the presence of high absorbing or high scattering phases that

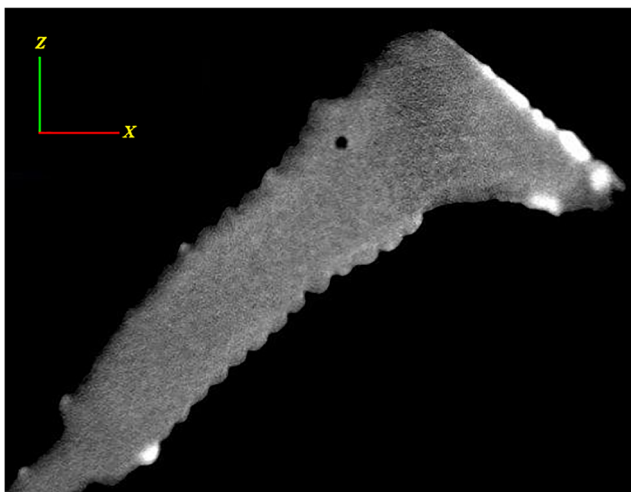


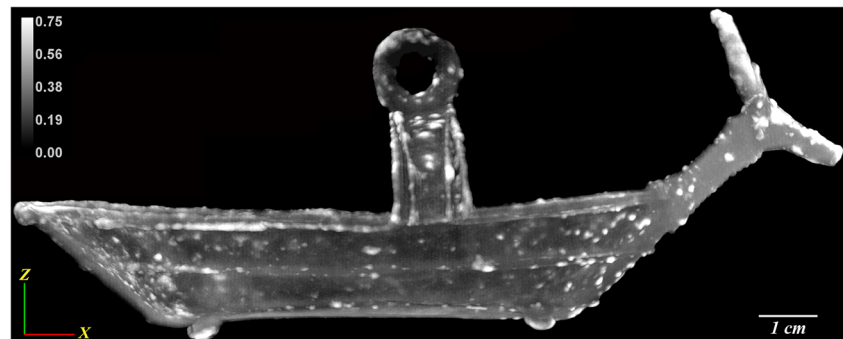
**Fig. 5** Slice of the *protome* taken in the XZ plane. Around the pore, it is possible to see dendrites, as intermixed lighter and darker areas. This presence is very important for the experiment since it testifies that the result from NT and ND agree

attenuate the beam. Table 2 reports the linear attenuation coefficient (LAC) for some alteration phases and for the constituents of bronze. The comparison of the values in the table with the calibration bar reported in the figure (which ranges from 0 to 0.75) suggests that the brightest points, which have the maximum value of attenuation, correspond to the phases that have a high LAC, such as atacamite. Hydrogen, indeed, is characterized by high incoherent neutron scattering cross-section: that is why the interaction with the beam is prevalent, also when compared to high attenuation phases such as chlorine. It has to be said, finally, that hydrate phases like atacamite did not produce clear Bragg peaks in the diffraction pattern due to their low phase fraction, but their interaction with the beam is so significant that they can be observed in tomographies.

### Neutron diffraction

The multiphase analysis revealed the presence of two diffraction patterns of a copper-tin alloy at a different relative concentration (evidence of a dendritic structure due to

**Fig. 6** Projection of the boat on the XZ plane. Bright spots are visible, especially in the snout of the *protome*



segregation during cooling), lead and some secondary phases (Table 3). Due to the complex shape of the sample, some diffraction patterns showed unidentified peaks, most likely caused by an unwanted part of the boat being simultaneously irradiated by the neutron beam, producing additional spurious diffraction peaks, which were considered as background noise. Measuring samples with complex and hollow shapes is not an easy task, and a correct sample positioning is of fundamental importance to avoid multiple scattering effects. The boat is in a good conservation state, thanks to a recent restoration (a series of different type of baths was performed to prevent the formation of secondary phases), but from the multiphase analysis emerged that some alteration phases are present in a high amount: for example, nantokite, a copper chloride ( $\text{CuCl}$ ), is in some parts as high as 4% wt. Such a high value could be due to the permanence of the boat in a chlorine-rich environment (probably the site where the boat was found), the element that leads to the formation of nantokite. Nantokite is a highly corrosive phase that must be treated with corrosion inhibitor solutions to stop material degradation. In fact, this phase could lead to the formation of paratacamite, the hydrate form of chlorides, a very dangerous phase for the metal. Lead was found in very low concentrations in the structure, generally around the detection limit for this phase, which is 0.2 wt%

(Grazzi et al. 2007). Lead was usually added to facilitate casting, but, for this object, its presence is likely to be due to its occurrence in the ore used to refine copper or tin rather than as an intentional addition. With regard to the alloy characterization, the dendritic structure is modelled by two FCC structure  $\alpha$ -phases having lattice parameters that correspond to the shoulders of a structured diffraction pattern. The lattice parameter values vary throughout the sample, with an average value that is around  $3.659 \pm 0.004 \text{ \AA}$  and  $3.677 \pm 0.001 \text{ \AA}$ , respectively. The equivalent tin content is calculated from the lattice parameter of the alpha phases (Grazzi et al. 2007). The average Sn content of the  $\alpha$ -bronze phases was estimated to range from 8.0 to 10.4 wt%, and, as it is possible to see in Fig. 7, it varies distinctly within the boat structure. The keel, indeed, has a slightly lower amount of tin compared to the upper part of the hull (and the snout). The different tin amount is also visible in the diffraction pattern: Fig. 8 compares the measured area with the lowest tin concentration with the one with the highest tin concentration, showing a misalignment in the peak position that testifies a variation in the lattice parameter, and hence tin content. This means that, at the moment of casting, the mould was placed upwards, with the hull top facing the ground. Since tin is heavier than copper, as a consequence of gravity, the part of the molten metal rich in this element

**Table 2** Linear attenuation coefficient of some alteration phases and from the constituents of bronze. The value is calculated from the packing density, which is given by the product of the phase density times 0.5 (Sears 1992). The calculated values differ from the ones in

the grey bar: anyway, a high LAC corresponds to high attenuation of the beam. Furthermore, the hydrate fraction in secondary phases is not always constant, so the coefficient can vary. The LAC was calculated for a neutron wavelength of  $2.6 \text{ \AA}$

Phase		Packing density ( $\text{g/cm}^3$ )	Linear att. coefficient ( $\text{cm}^{-1}$ )
Nantokite	CuCl	1.92	0.91
Cuprite	Cu <sub>2</sub> O	3.05	0.23
Atacamite	Cu <sub>2</sub> Cl(OH) <sub>3</sub>	1.86	1.87
Covellite	CuS	2.38	0.23
Bronze	Pb	5.67	0.18
	Cu-Sn (90–10)	4.38	0.28

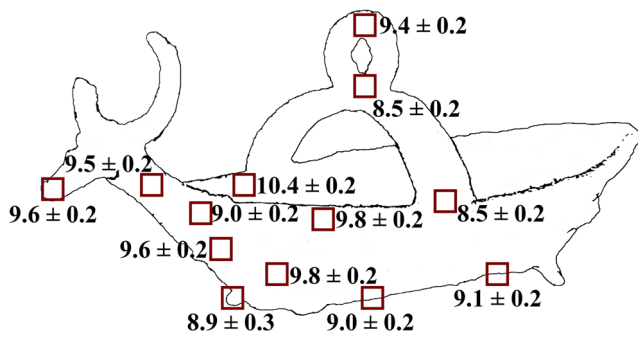
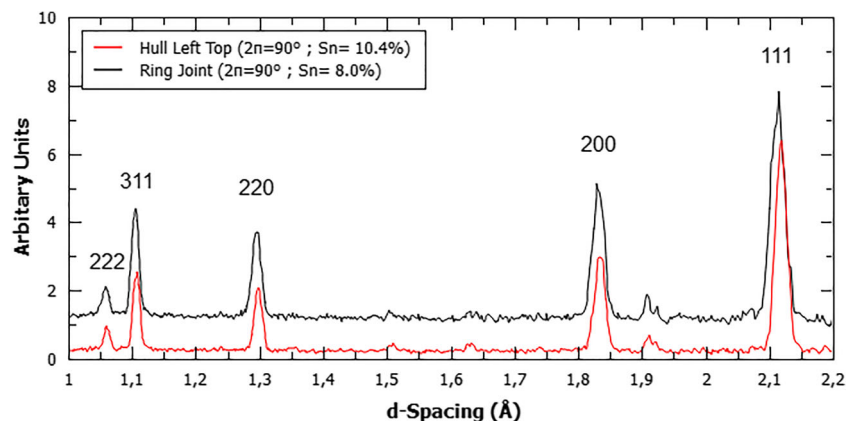


**Fig. 7** Percentage of calculated Sn (in the alloy) as weight fraction. Dotted lines refer to the measuring point on the bottom and the rear part of the hull

concentrated in the lower parts of the mould, corresponding to the hull top and the snout. Such type of casting was probably easier to control and execute; furthermore, it allowed to produce a thinner keel. Given the variation of the tin concentration in the hull, a constructive issue regards the bridge. The hull-bridge connection and the bridge-ring connection, indeed, are the two measured areas with the lowest average concentrations of tin, around 8.0–8.5 wt%, as shown in Fig. 7. This means that the bridge has a higher melting temperature than the hull: as a consequence, the bridge was not put in place with the cast-on method, because the high-temperature metal would have melted the connecting region in the hull top and created a poor connection. What emerges from the comparison of the imaging and diffraction data can be explained by hypothesizing that the bridge was cast before the hull and then put on top of the wax model of the boat. In this way, when the large mould for the boat main part was made, it would have included the pre-casted bridge: the connection was then created by the molten metal poured into the mould. In such a hypothesis, the bridge connection would have been external with respect to the hull, as it is possible to see in Fig. 4A. Eventually,

**Fig. 8** Copper alloy peaks from a tin-richer area (red pattern) are shifted towards higher d-spacings with respect to alloy peaks from a copper-richer part (black pattern)



the ring was placed on top of the bridge with the casting-on technique. Such a hypothesis is in agreement with the data from the tomography: the clearest discontinuities visible, indeed, correspond to the hull-bridge and the bridge-ring connection (discontinuities that make the artefact more fragile compared to an artefact made with a single cast). This type of manufacturing is a reliable method that can be deduced from a careful analysis of the imaging and diffraction data: furthermore, throughout the years, some pre-casted bridges were found at archaeological sites, suggesting the possibility that this type of practice was known among the metallurgists (Depalmas 2005). Eventually, manufacturing methods and thermal treatments leave characteristic microstructural features that usually can be detected by the analysis of the peak shape parameters, such as the Gaussian  $s_{400}$  and the Lorentzian broadening  $\gamma_2$  (Grazzi et al. 2007). The “lost wax” method, indeed, requires the casting mould to be pre-heated to prevent it from shattering when pouring the metal. The cast is then allowed to cool at a relatively slow rate due to the large mass of the mould and, after that, the artefact is removed from the clay and worked with some different tools (Lechtman and Steinberg 1980). In this work, due to the presence of dendrites which affect the peak shape and broadening in all the measuring points, it is not possible to give a valid interpretation of  $\gamma_2$  and  $s_{400}$  data: any assumption could be misrepresented by the lattice parameter displacement composition effect that prevails in the broadening of the peaks.

## Conclusions

A Sardinian bronze boat model was analysed by means of non-destructive neutron techniques. The main interest regarding the Colovros boat concerned the phase characterization and the manufacturing process. The object belongs

**Table 3** Characterization of the metallic and mineralization phases in weight concentration (wt%). The deviating alpha phase amounts of the ring joint and the hull bridge connection could be due to a process similar to annealing induced by the high-temperature molten metal poured into

the mould at the moment of the hull casting. The investigated area of each point was decided accordingly to the specific shape of the sample while the observed sample volume is given by the product of the measured area and its thickness

Position	Measured area (mm <sup>2</sup> )	$\alpha$ Cu-Sn		Pb	Cu <sub>2</sub> O	CuCl	Cu <sub>2</sub> S
		I	II				
Hull bow side	150	24.2 ± 0.8	71.5 ± 0.8	-	2.1 ± 0.1	2.2 ± 0.1	-
Hull stern side	150	44.8 ± 2.1	49.6 ± 2.1	0.4 ± 0.1	2.0 ± 0.1	2.5 ± 0.1	0.7 ± 0.2
Ring	30	36.4 ± 0.8	57.6 ± 0.8	0.3 ± 0.2	1.5 ± 0.1	3.5 ± 0.1	0.8 ± 0.3
Ring joint	20	72.8 ± 1.4	23.5 ± 1.4	0.3 ± 0.2	1.4 ± 0.1	2.1 ± 0.1	-
Hull right top	25	36.1 ± 1.9	57.8 ± 1.9	-	1.6 ± 0.1	2.1 ± 0.1	2.4 ± 0.4
Hull-bridge connection	10	82.6 ± 0.9	9.9 ± 0.9	-	1.6 ± 0.1	2.9 ± 0.1	2.9 ± 0.1
Hull left top	25	20.1 ± 2.4	75.2 ± 2.4	-	2.0 ± 0.2	2.5 ± 0.3	-
Foot bow side	25	43.2 ± 1.7	48.7 ± 1.7	0.8 ± 0.5	2.5 ± 0.2	4.8 ± 0.2	-
Hull right bottom	25	40.8 ± 1.1	54.8 ± 1.1	0.5 ± 0.2	1.6 ± 0.1	2.2 ± 0.1	-
Hull under neck	30	32.8 ± 0.5	64.1 ± 0.5	-	1.3 ± 0.1	1.8 ± 0.1	-
Hull neck joint	9	35.9 ± 1.8	59.6 ± 1.8	0.4 ± 0.1	1.8 ± 0.1	1.7 ± 0.1	0.6 ± 0.2
Neck	50	29.9 ± 1.4	65.1 ± 1.4	0.2 ± 0.1	1.6 ± 0.1	2.2 ± 0.1	0.9 ± 0.2
Snout	25	36.1 ± 1.5	55.4 ± 1.5	0.4 ± 0.3	2.3 ± 0.1	5.9 ± 0.2	-

to a group of relatively simple boat models, compared to technically more complex artefacts such as the one from Vetulonia. Our analysis has shown that the object was made through the assembly of separated cast parts. In fact, the boat is the sum of three different parts, connected together in a defined sequence: the bridge, cast a first; the hull, cast onto the bridge while oriented upside down; and the ring, cast on the top of the bridge. In this object, the casting was achieved in a different way from the Vetulonia one (Brunetti and Al 2018). The neutron diffraction data gave a clear identification of the alteration phases present in the bronze object, characterized by a relatively high amount of nantokite. Even though the boat was recently restored, it has to be stored in a dry environment to prevent the hydration of this phase, to avoid the formation of other copper chloride hydroxides and further alteration of the metal. Furthermore, the results obtained from neutron tomography confirm the microstructural characterization obtained from the neutron diffraction experiment. Data from multiple areas and spatially resolved results are further confirmation of the value of neutron-based techniques, especially when used together as demonstrated in this study which otherwise would have been only achievable using destructive analysis approaches.

**Acknowledgements** The cooperation Agreement no. 06/20018 between CNR and STFC, concerning collaboration in scientific research at the spallation neutron source ISIS (UK) and the *Regione Sardegna* (research project CUP J81G17000140002) Sviluppo di una metodologia

spettroscopica integrata e innovativa per la caratterizzazione di bronzi antichi is gratefully acknowledged.

**Code availability** Not applicable.

**Funding** Open access funding provided by Università degli Studi di Sassari within the CRUI-CARE Agreement.

**Data Availability** Not applicable.

## Declarations

**Conflict of interest** The authors declare that there is no conflict of interest.

**Open Access** This article is licensed under a Creative Commons Attribution 4.0 International License, which permits use, sharing, adaptation, distribution and reproduction in any medium or format, as long as you give appropriate credit to the original author(s) and the source, provide a link to the Creative Commons licence, and indicate if changes were made. The images or other third party material in this article are included in the article's Creative Commons licence, unless indicated otherwise in a credit line to the material. If material is not included in the article's Creative Commons licence and your intended use is not permitted by statutory regulation or exceeds the permitted use, you will need to obtain permission directly from the copyright holder. To view a copy of this licence, visit <http://creativecommons.org/licenses/by/4.0/>.

## References

Arnold O, Al (2014) Mantid data analysis and visualization package for neutron scattering and  $\mu$ SR experiments. Nuclear instruments and

- methods in physics research, section A: accelerators, spectrometers, detectors and associated equipment 764:156–166. <https://doi.org/10.1016/j.nima.2014.07.029>
- Brunetti A, Al (2018) Non-destructive microstructural characterization of a bronze boat model from Vetulonia. *Archaeol Anthropol Sci* 11(6). <https://doi.org/10.1007/s12520-018-0731-6>
- Celli M, Grazzi F, Zoppi M (2007) A new ceramic material for shielding pulsed neutron scattering instruments. *Nuclear instruments and methods in physics research section A* 565(2):861–863. <https://doi.org/10.1016/j.nima.2006.05.234>
- Depalmas A (2005) Le navicelle di bronzo della Sardegna nuragica. Collana la Terra dei Re, Ettore Gasperini Editore, Cagliari
- Depalmas A (2009) Il Bronzo medio, recente, finale in Sardegna. In: *La preistoria e la protostoria della Sardegna, I, Atti della XLIV Riunione Scientifica IIPP. IIPP, Firenze*, pp 123–160
- Depalmas A (2014) Le navicelle, in *La Sardegna nuragica. Storia e materiali. Corpora delle antichità della Sardegna*, Carlo Delfino, Roma, pp 121–136
- Depalmas A (2019) From collective tombs to individual burials: changes and transformations in Sardinian society over the second and first millennia BC. *Origini XLIII* 2020:141–160
- Depalmas A., Bulla C., Fundoni G. (2016) “I santuari nuragici: architettura, organizzazione e funzione degli spazi”, in A. Russo, F. Guarneri (a cura di), *Santuari mediterranei tra Oriente ed Occidente. Interazione e contatti culturali*, Roma 341–349
- Depalmas A., di Gennaro F., Sanciu A. (n.d.) “Una navicella bronzea dal territorio di Lula”, in *Studi in onore di GiuseppaTanda*, forthcoming
- Dierick M, Masschaele B, Hoorebeke LV (2014) Octopus, a fast and user-friendly tomographic reconstruction package developed in LabView. *Meas Sci Technol* 15:1366
- Grazzi F (2018) & Al. “Non-destructive compositional and microstructural characterization of Sardinian Bronze Age swords through neutron diffraction”. *Mater Charact* 144:387–392. <https://doi.org/10.1016/j.matchar.2018.07.035>
- Grazzi F, Celli M, Siano S, Zoppi M (2007) Preliminary results of the Italian neutron experimental station INES at ISIS: Archaeometric applications. *Il Nuovo Cimento* 30:59. <https://doi.org/10.1393/ncc/i2006-10039-5>
- Imberti S, Kockelmann W, Grazzi F et al (2008) “Neutron diffractometer INES for quantitative phase analysis of archaeological objects”. *Meas Sci Technol* 3:19. <https://doi.org/10.1088/0957-0233/19/3/034003>
- Kak AC (2001) Slaney M. *Society of Industrial and Applied Mathematics, Principles of computerized tomographic imaging*
- Kardjilov N., Festa G. (2017) *Neutron methods for archaeology and cultural heritage* Springer 7–11
- Kockelmann W. & Al (2018) Time-of-flight neutron imaging on IMAT@ISIS: a new user facility for materials science. *J Imaging* 4:47. <https://doi.org/10.3390/jimaging4030047>
- Larson AC VDRB (2004) *General structure analysis system (GSAS)*. Los Alamos National Laboratory Report LAUR:86–748
- Lechtman H., Steinberg A. (1980) “Bronze joining: a study” in W. A. Oddy *Aspects of early metallurgy*, British Museum Occasional Paper, British Museum London 17: 1–33
- McCusker LBM, Von Dreele RB, Cox DE, Louer D (1999) Rietveld refinement guidelines. *J Appl Crystallogr* 32:36–50
- Preibisch S, Saalfeld S, Tomancak P (2009) Globally optimal stitching of tiled 3D microscopic image acquisitions. *Bioinformatics* 11(25): 1463–1465. <https://dx.doi.org/10.1093%2Fbioinformatics%2Fbtp184>
- Ruenden CT, Al (2017) ImageJ2: ImageJ for the next generation of scientific image data. *BMC Bioinformatics* 18:529. <https://doi.org/10.1186/s12859-017-1934-z>
- Sears VF (1992) *Neutron News* 3(3):29–37
- Toby BH (2001) EXPGUI, a graphical user interface for GSAS. *J Appl Crystallogr* 34:210–213. <https://doi.org/10.1107/S0021889801002242>

**Publisher's note** Springer Nature remains neutral with regard to jurisdictional claims in published maps and institutional affiliations.